NANO LETTERS

Letter

pubs.acs.org/NanoLett

Motion Transduction in Nanoelectromechanical Systems (NEMS) Arrays Using Near-field Optomechanical Coupling

O. Basarir,[†,‡,∥] S. Bramhavar,[‡,§] and K. L. Ekinci*[,†,‡]

[†]Department of Mechanical Engineering, [‡]The Photonics Center, and [§]Department of Electrical and Computer Engineering, Boston University, Boston, Massachusetts, 02215, United States

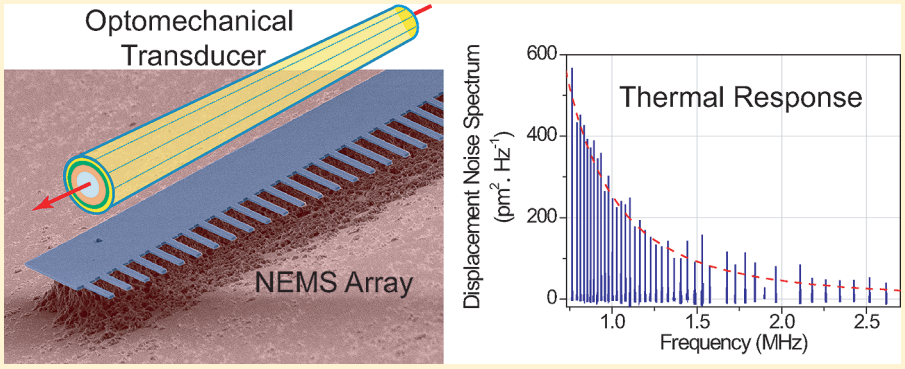

ABSTRACT: Development of efficient and sensitive motion transducers for arrays of nanoelectromechanical systems (NEMS) is important for fundamental research as well as for technological applications. Here, we report a single-wire nanomechanical transducer interface, which relies upon near-field optomechanical interactions. This multiplexed transducer interface comes in the form of a single-mode fiber taper on a fiber-optic cable. When the fiber taper is positioned sufficiently close to the NEMS array such that it can attain evanescent optical coupling with the array, individual NEMS resonances can be actuated using optical dipole forces. In addition, sensitive detection of nanomechanical motion can be realized when the evanescent waves confined around the taper are scattered by the motion. We have measured resonances from an array of 63 NEMS resonators with a displacement sensitivity of 2−8 pm·Hz$^{-1/2}$ at a detection power of ∼100 μW (incident on the entire array).

KEYWORDS: *NEMS arrays, optomechanics, optomechanical transducer, nanomechanics, fiber taper, near-field interactions*

Nanoelectromechanical systems (NEMS)-based fundamental metrology[1,2] and technological applications[3−8] are poised to benefit from the development of efficient and sensitive nanomechanical transducers. This is because useful signals are encoded in nanomechanical motion in a typical sensing or measurement endeavor involving a NEMS resonator. Exciting and measuring the small NEMS motion at low input power levels and with as little added noise as possible, therefore, remains of paramount importance to the NEMS community. Impressive nanomechanical displacement sensitivities have been achieved by exploiting both optical,[9−15] and electronic[1,2,16−22] phenomena. Much of the reported work, however, remains on single NEMS resonators with a few notable exceptions.[19,23−25] Yet, it is clear that arraying NEMS devices at the chip scale will be the way of the future. What is needed, therefore, is an efficient multiplexed transducer for NEMS arrays, which preferably comes in the form of a seamless single-wire interface.

In this article, we describe such an optical transducer technology for NEMS arrays. Our transducer is based upon near-field (evanescent) optical interactions. Near-field optical interactions suit the NEMS domain well because they are typically not limited by diffraction. Both actuation[9,12,24,26] and sensing[9,11−13,24−29] of NEMS motion have been realized using near-field interactions with modest coherence and stability requirements. Our array transducer, which is based on a fiber taper, aims to circumvent some of the imitations encountered in earlier NEMS array work, such as free-space optical components,[24,25] off-chip circuit components,[19] magnetic field requirements,[23] requirements for high-index materials[24] and so on. First and foremost, the taper provides a *single-wire multiplexed transduction interface* between the NEMS chip and the measurement equipment. Because the taper can easily be fabricated on a fiber optic cable, our approach obviates the need for free-space optics and is straightforward to implement. This simple off-chip transducer can be fully integrated for large-scale distributed NEMS arrays by replacing the fiber taper with an on-chip waveguide. Finally, the transducer provides high displacement sensitivity and actuation efficiency at low optical power levels.

Figure 1a shows an illustration of our single-wire interface and the block diagram of the measurement setup. Our transducer comes in the form of a fiber taper; the taper has a

Received: May 17, 2011
Revised: January 12, 2012
Published: January 19, 2012

   dx.doi.org/10.1021/nl2031585 | *Nano Lett.* 2012, 12, 534−539

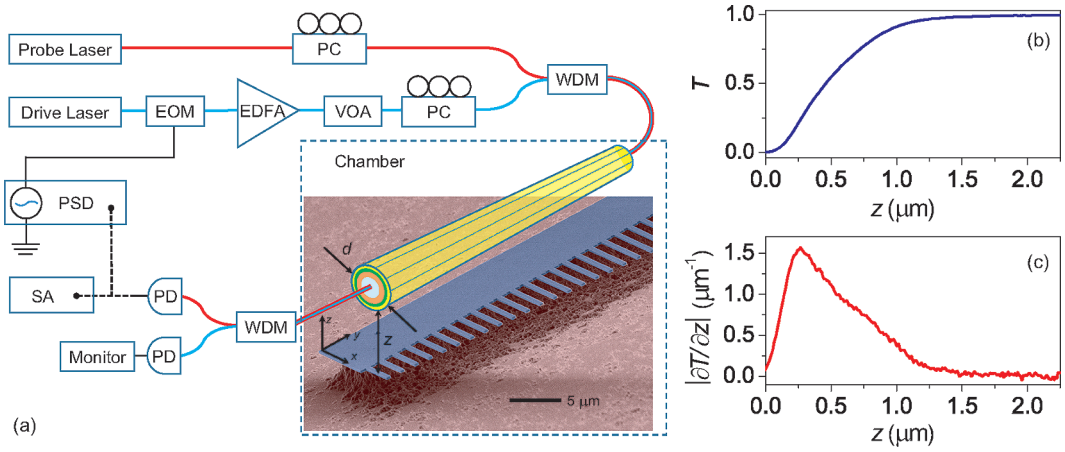

Figure 1. (a) Schematic of the experimental setup superimposed on the SEM image of a NEMS cantilever array. Light from two different diode lasers is combined in a pump−probe scheme and directed into the fiber taper. The transmitted light is separated by wavelength and the probe portion is sent onto a high-speed photodetector (PD). The actuation circuit comprises of an electro-optic intensity modulator (EOM), an erbium-doped fiber amplifier (EDFA), variable optical attenuators (VOA), fiber polarization controllers (PC), and wavelength division multiplexers (WDM). A spectrum analyzer (SA) is used for noise measurements; phase-sensitive detection (PSD) using a network analyzer is employed to measure the driven response. (b,c) Normalized optical transmission T and its numerically calculated derivative $|\partial T/\partial z|$ as a function of the taper-device separation z, respectively.

diameter of $d \approx 1$ μm. The fiber taper is positioned above the NEMS array by a distance z using calibrated stages. Low-frequency drifts of the taper during measurements are nulled using a digital feedback loop. All the measurements are performed in a custom built variable pressure chamber with a base pressure $p \approx 2 \times 10^{-2}$ Pa. Two tunable laser sources operating in the telecom band are used for detection and actuation. The output of the actuation laser is intensity modulated using a commercial $LiNbO_3$ modulator and amplified with an erbium-doped fiber amplifier (EDFA) before entering the input coupler. In our approach, the displacement sensing mechanism is based on the scattering of evanescent optical waves localized outside the taper.[28−30] Optical dipole forces due to the field gradients around the taper allow for actuation of nanomechanical motion.[12,24,26,27,31]

The resonator arrays are patterned on a silicon-on-insulator (SOI) wafer (with a sacrificial SiO_2 layer of 3 μm) using standard electron-beam lithography and a fluorine based plasma etch. In order to isolate the mechanical devices from the rest of the chip, a mesa structure is defined using optical lithography followed by deep silicon etching. Finally, the devices are released by a hydrofluoric acid (HF) vapor etch. The undercut of the cantilevers in the array is ∼1 μm.

The Si NEMS resonators in the array scatter the evanescent tail around the fiber-taper when the taper is positioned sufficiently close to the NEMS array. This reduces the transmission T of the taper.[29,30] For small oscillations of the N individual resonators in the array as well as the taper, the optical power $P_{pd}(t)$ detected on the photodetector can be expressed as[32]

$$P_{pd}(t) \approx P_{in}\left[T(z_0) + \left|\frac{\partial T}{\partial z}\right|_{z=z_0} \delta z_f(t) + \frac{1}{N}\left|\frac{\partial T}{\partial z}\right|_{z=z_0} \sum_{n=1}^{N} \delta z_n(t)\right] \quad (1)$$

Here, P_{in} is the incident (probe) power on the fiber taper; the z-derivative of the transmission, $|\partial T/\partial z|$, is evaluated at the static gap value $z = z_0$; $\delta z_f(t)$ and $\delta z_n(t)$ are the time-dependent oscillation amplitudes of the taper and the n^{th} nanomechanical resonator, respectively. Assuming that the oscillation frequencies of the individual resonators are well-separated, nanomechanical motion can be detected[30] by simply monitoring the high-frequency spectrum of P_{pd} in a narrow band. The detection mechanism is insensitive to the phase of the light and can therefore be implemented using inexpensive incoherent light sources.[29]

In order to apply the above displacement detection principle to a NEMS array, we first measure the transmission T though the fiber taper as a function of the gap z between the array plane and the taper. In the experiment, we use a NEMS array comprised of 63 cantilever beams; the shortest 20 cantilevers in the array are shown in the scanning electron microscope (SEM) image of Figure 1a. The lengths of the cantilevers vary from 5 μm $\leq l_n \leq$ 18.8 μm, while the widths and thicknesses are equal for all: w = 500 nm and t = 230 nm, respectively. The variation in the length along with the typically high quality-factor of NEMS resonators ensures that the resonance frequencies will be well-separated. The fiber is first aligned to the tips of the cantilevers; it is subsequently brought toward the array plane while P_{pd} is monitored in a dc measurement. The resulting T versus z curve is shown in Figure 1b. The transmission is normalized to unity when the taper is far above the device. T decreases monotonically with decreasing z, except in the final ∼5 nm of the approach when the fiber snaps to contact accompanied by an abrupt change in T. The zero gap is taken as the z value where $T \approx 1 \times 10^{-4}$; however, the exact location of the zero gap is not important since the transducer is typically operated far from the zero gap limit. The slope of the transmission curve with respect to the gap, $|\partial T/\partial z|$, is shown in the Figure 1c. This slope along with the array size N determines the inverse displacement detection responsivity per (individual) resonator, $(1/N)|\partial T/\partial z|$, as expressed in eq 1 above. It is worth noticing that $|\partial T/\partial z|$ shown in Figure 1c has a well-defined maximum at $z \approx$ 270 nm. This maximum emerges because of two competing effects as z is reduced: the evanescent coupling increases while the transmitted power decreases. Using the

dx.doi.org/10.1021/nl2031585 | Nano Lett. 2012, 12, 534−539

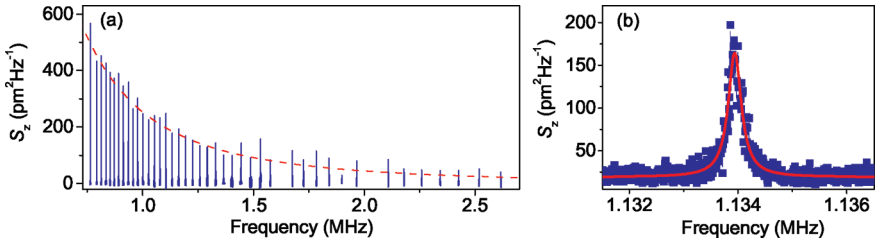

Figure 2. (a) Thermal noise spectra (backgrounds subtracted) for the first 42 cantilevers along with the theoretically expected envelope (red dashed line) proportional to $f^{-5/2}$. (b) Representative thermal noise peak (blue) for one cantilever having dimensions $l \times t \times w$ = 15.6 μm × 230 nm × 500 nm and stiffness of $k \approx 6 \times 10^{-2}$ N·m^{-1}. The solid line is a fit to a Lorentzian line-shape with a resonance frequency of $f \approx 1.13$ MHz and a quality factor of $Q \approx 3800$. A displacement responsivity of $R \approx 1.2 \times 10^{-3}$ m·V^{-1} is obtained by using the approach outlined in the main text with the device parameters. This gives a measurement noise floor of $S_z^{1/2} \approx 4$ pm·Hz$^{-1/2}$ for this device.

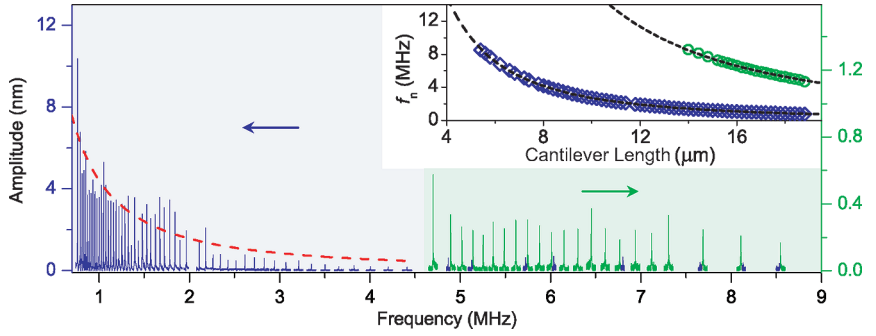

Figure 3. Optically actuated response showing measured displacements of 63 cantilevers taken with an actuation power of 50 μW and a probe power of 100 μW. The blue (green) spectra correspond to fundamental (first harmonic) flexural resonances. The dashed red line is proportional to $f^{-3/2}$ and is calculated from the device geometry and material properties of the resonators. The inset shows the expected (dashed line) and measured resonance frequencies of both the fundamental (diamonds) and first harmonic (circles) resonances as a function of cantilever length.

maximum value of $|\partial T/\partial z|$ one obtains $(1/N)|\partial T/\partial z| \approx 0.024$ μm^{-1}; this value provides the maximum displacement detection sensitivity for each element of the array as discussed in more detail below.

For displacement detection, we position the fiber taper at the maximum sensitivity point, $z \approx 270$ nm, found in the dc transmission measurements. We then monitor the spectrum of the transmitted power using a spectrum analyzer. Figure 2a displays the high-frequency spectrum of the noise measured on the array with $P_{in} \approx 100$ μW. Well-separated thermal peaks from the fundamental out-of-plane resonances of the first 42 cantilevers are noticeable. These thermal peaks provide a reliable calibration for the displacement detector (see below). Each individual resonator n exhibits a thermal peak with a Lorentzian line-shape, such as the one shown in Figure 2b. The measured resonance frequencies and quality factors are 0.75 MHz $\leq f_n \leq$ 2.6 MHz and 3500 $\leq Q_n \leq$ 6000. Not shown are the two orthogonal low-frequency modes of the fiber taper itself[30] at $f_f^l \approx 2.548$ kHz and $f_f^u \approx 2.555$ kHz. The particular fiber (with transmission loss of ~1.5 dB) used in this work has a spring constant of $k_f \approx 0.74 \times 10^{-3}$ N·m^{-1}, resulting in an rms thermal amplitude of $\langle \delta z_f^2 \rangle^{1/2} \approx 2.3$ nm. This stiffness k_f is smaller than that of most of the cantilevers in the array. However, it is large enough that the deflections of the fiber induced by optical and van der Waals forces can be neglected,[29] except when the gap is very small, $z \sim 5$ nm.

In order to calibrate the oscillation amplitudes, we assume that each NEMS resonator in the array can be described as a one-dimensional damped harmonic oscillator with stiffness k_n, effective mass m_n, and mechanical resonance frequency f_n. Also implicit is the relation $k_n = m_n\omega_n^2$, where $\omega_n = 2\pi f_n$. Given the displacement noise spectral density $S_{z_n}(f)$, the equipartition theorem provides the mean-square displacement $\langle \delta z_n^2 \rangle$ of the n^{th} mechanical resonator as $\langle \delta z_n^2 \rangle = \int_0^\infty S_{z_n}(f)\mathrm{d}f = (k_B\theta)/(k_n)$. Here, k_B is the Boltzmann constant and θ is the absolute temperature. In the experiments, a voltage due to the motion of a resonator is measured. For calibration, we need the overall displacement responsivity R_n (in units of m·V^{-1}); this can then be used to convert any voltage to a displacement or vice versa. The calibration procedure is as follows: The voltage noise spectral density $S_{V_n}(f)$ (in units of V^2·Hz^{-1}) of an undriven resonator is measured as a function of frequency at the output. R_n is extracted from $R_n^2 = (k_B\theta/k_n)/(\int_0^\infty S_{V_n}(f)\mathrm{d}f)$ using the measured S_{V_n}, calculated k_n and the ambient temperature values. This calibration procedure is valid for a given optical probe power and taper-resonator separation and is repeated for each device. The minimum attainable displacement sensitivity can be expressed as $S_{z_n}^{1/2} = R_n S_{V_n}^{1/2}$. The dominant noise mechanism in our setup is the laser intensity noise. At this limit, 2 pm·Hz$^{-1/2}$ $\leq S_{z_n}^{1/2} \leq$ 8 pm·Hz$^{-1/2}$. Ideally, the detector should provide the same displacement sensitivity for all the individual resonators in the array since the responsivity R_n depends upon the scattered light, which is only a function of the individual resonator width.[30] In reality, however, R_n varies by 30% among resonators. The variation observed is due to the nonuniform noise floor in the relatively broad frequency band of the measurement and the slight misalignment of the fiber taper with respect to the resonators. In addition, the undercut of the structures affects the calibration because of k_n; R_n varies by 15% from its nominal value. Finally, returning to eq 1, we note that the R_n's found from the thermal calibration agree to within 20% with those obtained independently from the transmission (T versus z) curve of Figure 1b . In this approach, the R_n's are

dx.doi.org/10.1021/nl2031585 | Nano Lett. 2012, 12, 534–539

found using $(1/N)(|\partial T/\partial z|)$ (after accounting for the responsivity and gain of the photodetector). This close agreement gives us confidence that the approximation in eq 1 describes the displacement sensor well.

The dashed envelope curve in Figure 2a, proportional to $f^{-5/2}$, is a theoretical fit to the experimentally measured $S_{z_n}(f)$ values using an average quality factor for the whole array. The measured rms displacements and hence $S_{z_n}(f)$ decrease at higher frequencies due to the increased stiffness. For the n^{th} device, the displacement noise spectral density $S_{z_n}(f)$ at $f = f_n$ simplifies to

$$S_{z_n}(f_n) = \frac{4k_B\theta Q_n}{m_n(2\pi f_n)^3} \tag{2}$$

The effective mass m_n for the fundamental (out-of-plane) flexural mode of a cantilever with linear dimensions $l_n \times w \times t$ and density ρ can be calculated as $m_n = 0.25\rho wtl_n$; the resonance is at a frequency $f_n = (\omega_n/2\pi) = 0.162(E/\rho)^{1/2}(t/l_n^2)$, where E denotes the Young's modulus. Realizing that only the length l_n changes for array elements and using the relations for m_n and f_n, one obtains

$$S_{z_n}(f_n) = 0.161\beta k_B\theta\frac{Q_n}{f_n^{5/2}} \tag{3}$$

where $\beta = (wE^{1/4}\rho^{3/4}t^{3/2})^{-1}$ (in $\text{kg}^{-1}\cdot\text{s}^{1/2}$). The measured Q_n remain in the range $3500 \leq Q_n \leq 6000$. If one simply assumes an average quality factor of $\overline{Q_n} \approx 4500$ for all the resonators in the array and uses E and ρ for Si along with the device dimensions, one obtains the envelope in Figure 2a.

In Figure 3, the driven response of the NEMS array is shown. In these measurements, experimental parameters such as the fiber taper position, dc light levels and polarization states are optimized and kept as close as possible to the thermal noise measurements for a reliable displacement calibration. Using the same fiber taper, a second intensity-modulated laser source is used to resonantly excite devices through the optical gradient force. The intensity modulation signal is provided by a network analyzer. The excitation path originating from the intensity modulated laser is shown in blue in Figure 1a. The entire array is driven by an optical power of 50 μW (in addition to the probe power of $P_{\text{in}} \approx 100$ μW) at $z \approx 270$ nm. The detection is performed as described above. The peaks observed in Figure 3 correspond to all the fundamental flexural resonances of the 63 cantilevers in the array along with a number of first harmonics of the softer cantilevers. The decrease of resonance amplitudes at higher frequencies can be attributed both to higher stiffness and to slight misalignments of the taper. The inset to Figure 3 displays the dependence of resonance frequency f_n on the device length l for all the measured fundamental (diamonds) and first harmonic (circles) modes.[33]

The displacement calibration is obtained from the thermomechanical motion of the 42 cantilevers shown in Figure 2a. As discussed above, first the responsivity R_n is obtained for each resonator separately. For driven motion, $\delta\widetilde{z}_n(f) = R_n\widetilde{V}_n(f)$ where $\delta\widetilde{z}_n(f)$ is the rms displacement amplitude of the n^{th} resonator and $\widetilde{V}_n(f)$ is the rms voltage measured at the drive frequency f. The on-resonance magnitude of the optical force driving the n^{th} resonator can then be found from $F_n = k_n\delta\widetilde{z}_n(f_n)/Q_n$ with Q_n obtained from the resonance line-shape and k_n from elasticity theory.

It is a good approximation to assume that the dropped actuation power and hence the actuation force on each cantilever in the array is the same, given that the width of the cantilevers are identical. In order to support this statement, we have calculated the envelope curve in Figure 3. The calculation uses identical considerations as above and results in the following on-resonance amplitude $\delta\widetilde{z}_n(f_n)$ for driven motion

$$\delta\widetilde{z}_n(f_n) = 0.25\beta F_n\frac{Q_n}{f_n^{3/2}} \tag{4}$$

Taking an average $\overline{Q_n} \approx 4500$, the best fit provides $F_n = 45$ fN. The slight discrepancy between the data and the fit is mainly due to fact that Q_n and F_n are assumed the same for each resonator. Furthermore, as discussed above the uncertainty in R_n also propagates into the calculations. We have also determined from finite element method (FEM) simulations that when the array is excited at frequency f_n, there is negligible mechanical coupling between devices and the majority of the mode energy stays within the n^{th} device.

We now discuss the temperature rises induced by our transducer. First, when a mechanical resonator interacts with a nearby fiber taper, it absorbs some of the optical power from the taper. In vacuum, this is expected to generate a localized temperature rise on the device; heat is subsequently conducted to the clamps. Neglecting scattering effects and assuming that the device absorbs all the power the taper loses, an upper limit for the local temperature rise can be estimated. Due to the high aspect ratio of the mechanical device $(l/w, l/t \gg 1)$, a one-dimensional temperature distribution, $\theta_n(x)$ (see coordinate axes in Figure 2a) can be assumed. For a single cantilever with heat flux q'' at the free-end,[34] the maximum temperature is found as $\theta_n(l) = (q''l/\kappa) + \theta_c$, where κ is the thermal conductivity of the device and the clamp is at θ_c ($\theta_c \approx 300$ K). For a device of width $w = 500$ nm with 1.5 μW of dropped power ($P_{\text{in}} \approx 100$ μW) and an absorption rate[12] of $\alpha \approx 0.2$ $\text{dB}\cdot\text{cm}^{-1}$, we find an absorbed power of $P_a \approx 3.5$ pW over the width of the device. Thus, the heat flux is $q'' \approx (P_a/wt)$ where $w \times t$ is the cross-sectional area. This expression results in a temperature increase of $\Delta\theta_n \approx 4$ μK at the tip of the longest cantilever with $l \times w \times t = 18.8$ μm $\times$ 500 nm $\times$ 230 nm and will be smaller for the others. Second, an upper limit for the temperature rise of the isolated fiber taper can also be found by assuming that all the lost optical power is absorbed by it. Since the length L of the taper is much larger than its diameter, a one-dimensional model can be used. Using typical κ and α values for silica, and the fiber dimensions of $L \approx 1$ mm and $d \approx 1$ μm, we obtain an absorbed power of 7 pW (for a probe power of $P_{\text{in}} \sim 100$ μW). This leads to a temperature increase $\Delta\theta_f \approx 1$ mK around the center of the taper. When operating in a fluid such as air, the temperature rise in both the fiber taper and the cantilever are expected to be smaller.

Some future applications require that the single-wire transducer interface work well in an ambient environment.[35] In order to demonstrate this capability, we measure the resonant response of single NEMS resonators using the same measurement configuration under atmospheric pressure. The NEMS resonators here are doubly clamped beams and the fiber taper is aligned perpendicular to the length of the beam approximately at its center.[30] Figure 4a shows the thermal noise spectrum measured for a $w = 1000$ nm doubly clamped beam resonator using a probe power of ~100 μW at a gap $z \approx 75$ nm.

dx.doi.org/10.1021/nl2031585 | Nano Lett. 2012, 12, 534–539

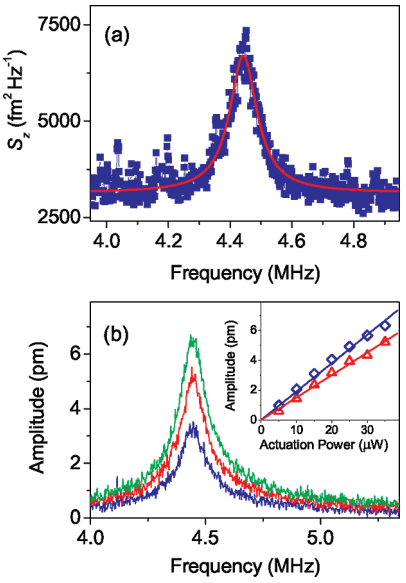

Figure 4. (a) Thermal peak of a doubly clamped beam resonator with $l \times t \times w$ = 15 μm × 230 nm × 1000 nm measured in air at the same probe power ($P_{in} \approx 100$ μW) at a gap $z \approx 75$ nm. A broadening in the peak is observed due to fluidic damping ($Q \approx 40$), whereas the resonance frequency does not change significantly from its vacuum value. At this power level and separation, a displacement sensitivity of $S_z^{1/2} \approx 56$ fm·Hz$^{-1/2}$ is obtained. (b) Optically driven response of the same device for three different actuation powers of 15, 25, and 35 μW. The inset shows the linear dependence of the NEMS amplitude on the actuation power at two different separations, 75 nm (diamonds) and 150 nm (triangles).

At this power level and separation, a displacement sensitivity of $S_z^{1/2} \approx 56$ fm·Hz$^{-1/2}$ is obtained. This increased displacement sensitivity is mainly due to the fact that the single NEMS beam interacts with most of the power incident on the fiber taper, as opposed to arrayed resonators where the power is shared between N beams. Furthermore, under atmospheric pressure, the taper can handle more optical power (up to ~5 mW) without failure, leading to increased detection sensitivity. We note that, in the case of a single NEMS resonator, we do not observe a maximum in the transmission T versus gap z curve. Rather, an exponentially decaying T versus z curve is obtained with a monotonically increasing $|\partial T/\partial z|$.[30] In Figure 4b, we display the optically driven resonances of the same device with the expected linear relation extracted in the inset. We notice no degradation in the coupling for either the detection or the actuation under atmospheric pressure.

As presented, the technique here is simple to implement for quick off-chip interrogation of a NEMS array. It could be improved in several respects. First, as encountered in past arrayed NEMS work,[19,23,24] it is not possible to multiplex signals from different resonators if their resonance frequencies are not well-separated. To the best of our knowledge, the only NEMS array read-out, where degenerate frequencies in the array could be resolved, is based on full-field free-space optical detection.[25] Here, this issue could be solved by perhaps relying on scattered (detected) power levels by fabricating resonators with the same frequency but different scattering cross sections, for example, fabricated out of different materials or different coatings.[36] This way degenerate resonators could be identified based on detected light levels. Second, a more robust device could be achieved by securing the fiber taper to on-chip support structures.[31] Alternatively, a separate waveguide chip could be bonded[37] to the NEMS chip or a buried channel waveguide could be fabricated under the device layer.[38] Finally, the displacement sensitivity could be further enhanced by employing shorter wavelength light sources or smaller, higher index waveguides. The resonator material is also not limited to high index dielectrics and could be replaced by metals or polymers.[39] In short, with such advances, the technique demonstrated here could be useful in a variety of new technological applications.

AUTHOR INFORMATION

Corresponding Author

*E-mail: ekinci@bu.edu.

Present Address

[‖]Fakultät für Physik and Center for NanoScience (CENS), Ludwig-Maximilians-Universität, Geschwister-Scholl-Platz 1, 80539 München, Germany.

Notes

The authors declare no competing financial interest.

ACKNOWLEDGMENTS

The authors acknowledge support from the U.S. National Science Foundation (NSF) through Grants ECCS-0643178, CBET-0755927, and CMMI-0970071. O.B. was partially supported by a Boston University Photonics Center Fellowship.

REFERENCES

(1) O'Connell, A. D.; Hofheinz, M.; Ansmann, M.; Bialczak, R. C.; Lenander, M.; Lucero, E.; Neeley, M.; Sank, D.; Wang, H.; Weides, M.; Wenner, J.; Martinis, J. M.; Cleland, A. N. Quantum ground state and single-phonon control of a mechanical resonator. *Nature* **2010**, *464*, 697.

(2) Hertzberg, J. B.; Rocheleau, T.; Ndukum, T.; Savva, M.; Clerk, A. A.; Schwab, K. C. Back-action-evading measurements of nanomechanical motion. *Nat. Phys.* **2010**, *6*, 213.

(3) Naik, K.; Hanay, M. S.; Hiebert, W. K.; Feng, X. L.; Roukes, M. L. Towards single-molecule nanomechanical mass spectrometry. *Nat. Nanotechnol.* **2009**, *4*, 445.

(4) Waggoner, P. S; Varshney, M.; Craighead, H. G. Detection of prostate specific antigen with nanomechanical resonators. *Lab Chip* **2009**, *9*, 3095.

(5) Gil-Santos, E.; Ramos, D.; Martinez, J.; Fernandez-Regulez, M.; Garcia, R.; Paulo, A. S.; Calleja, M.; Tamayo, J. Nanomechanical mass sensing and stiffness spectrometry based on two-dimensional vibrations of resonant nanowires. *Nat. Nanotechnol.* **2010**, *5*, 641.

(6) Lee, T.-H.; Bhunia, S.; Mehregany, M. Electromechanical computing at 500 degrees C with silicon carbide. *Science* **2010**, *329*, 1316.

(7) Blick, R. H.; Qin, H.; Kim, H.-S.; Marsland, R. A nanomechanical computer-exploring new avenues of computing. *New J. Phys.* **2007**, *9*, 241.

(8) Arlett, J.; Myers, E.; Roukes, M. Comparative advantages of mechanical biosensors. *Nature Nanotechnol.* **2011**, *6*, 203–215.

(9) Anetsberger, G.; Arcizet, O.; Unterreithmeier, Q. P.; Riviere, R.; Schliesser, A.; Weig, E. M.; Kotthaus, J. P.; Kippenberg, T. J. Near-field cavity optomechanics with nanomechanical oscillators. *Nat. Phys.* **2009**, *5*, 909.

(10) Liu, N.; Giesen, F.; Belov, M.; Losby, J.; Moroz, J.; Fraser, A. E.; McKinnon, G.; Clement, T. J.; Sauer, V.; Hiebert, W. K.; Freeman, M. R. Time-domain control of ultrahighfrequency nanomechanical systems. *Nat. Nanotechnol.* **2008**, *3*, 715.

(11) Eichenfield, M.; Camacho, R.; Chan, J.; Vahala, K. J.; Painter, O. A picogram- and nanometre-scale photonic-crystal optomechanical cavity. *Nature* **2009**, *459*, 550.

(12) Li, M.; Pernice, W. H. P.; Xiong, C.; Baehr-Jones, T.; Hochberg, M.; Tang, H. X. Harnessing optical forces in integrated photonic circuits. *Nature* **2008**, *456*, 480.
(13) Srinivasan, K.; Miao, H.; Rakher, M. T.; Davanço, M.; Aksyuk, V. Optomechanical Transduction of an Integrated Silicon Cantilever Probe Using a Microdisk Resonator. *Nano Lett.* **2011**, *11*, 791−797.
(14) Li, M.; Pernice, W. H. P.; Tang, H. X. Reactive cavity optical force on microdiskcoupled nanomechanical beam waveguides. *Phys. Rev. Lett.* **2009**, *103*, 223901.
(15) Pernice, W. H. P.; Li, M.; Tang, H. X. Optomechanical coupling in photonic crystal supported nanomechanical waveguides. *Opt. Express* **2009**, *17*, 12424−12432.
(16) Etaki, S.; Poot, M.; Mahboob, I.; Onomitsu, K.; Yamaguchi, H.; van der Zant, H. S. J. Motion detection of a micromechanical resonator embedded in a d.c. squid. *Nat. Phys.* **2008**, *4*, 785.
(17) Chen, S.; Rosenblatt, K. I.; Bolotin, W.; Kalb, P.; Kim, I.; Kymissis, H. L.; Stormer, T. F.; Heinz.; Hone, J. Performance of monolayer graphene nanomechanical resonators withelectrical readout. *Nat. Nanotechnol.* **2009**, *4*, 861.
(18) Regal, A.; Teufel, J. D.; Lehnert, K. W. Measuring nanomechanical motion with a microwave cavity interferometer. *Nat. Phys.* **2008**, *4*, 555.
(19) Truitt, P. A.; Hertzberg, J. B.; Huang, C. C.; Ekinci, K. L.; Schwab, K. C. Efficient and Sensitive Capacitive Readout of Nanomechanical Resonator Arrays. *Nano Lett.* **2007**, *7*, 120.
(20) Unterreithmeier, Q. P.; Weig, E. M.; Kotthaus, J. P. Universal transduction scheme for nanomechanical systems based on dielectric forces. *Nature* **2009**, *458*, 1001.
(21) Masmanidis, S. C.; Karabalin, R. B.; De Vlaminck, I.; Borghs, G.; Freeman, M. R.; Roukes, M. Multifunctional nanomechanical systems via tunably coupled piezoelectricactuation. *Science* **2007**, *317*, 780.
(22) Sazonova, V.; Yaish, Y.; Ustunel, H.; Roundy, D.; Arias, T. A.; McEuen, P. L. A tunable carbon nanotube electromechanical oscillator. *Nature* **2004**, *431*, 284.
(23) Venstra, W. J.; van der Zant, H. S. J. Efficient readout of micromechanical resonator arrays in ambient conditions. *Appl. Phys. Lett.* **2008**, *93*, 234106.
(24) Li, M.; Pernice, W. H. P.; Tang, H. X. Broadband all-photonic transduction of nanocantilevers. *Nat. Nanotechnol.* **2009**, *4*, 377.
(25) Sampathkumar, A.; Ekinci, K. L.; Murray, T. W. Multiplexed Optical Operation of Distributed Nanoelectromechanical Systems Arrays. *Nano Lett.* **2011**, *11*, 1014−1019.
(26) (a) Li, M.; Pernice, W. H. P.; Tang, H. X. Tunable bipolar optical interactions between guided lightwaves. *Nat. Photonics* **2009**, *3*, 464−468. (b) Roels, J.; De Vlaminck, I.; Lagae, L.; Maes, B.; Van Thourhout, D.; Baets, R. Tunable optical forces between nanophotonic waveguides. *Nat. Nanotechnol.* **2009**, *4*, 510.
(27) Wiederhecker, G. S.; Chen, L.; Gondarenko, A.; Lipson, M. Controlling photonic structures using optical forces. *Nature* **2009**, *462*, 633.
(28) Vlaminck, D.; Roels, J.; Taillaert, D.; Thourhout, D. V.; Baets, R.; Lagae, L.; Borghs, G. Detection of nanomechanical motion by evanescent light wave coupling. *Appl. Phys. Lett.* **2007**, *90*, 233116.
(29) Basarir, O.; Bramhavar, S.; Basilio-Sanchez, G.; Morse, T.; Ekinci, K. L. Sensitive micromechanical displacement detection by scattering evanescent optical waves. *Opt. Lett.* **2010**, *35*, 1792.
(30) Basarir, O.; Bramhavar, S.; Ekinci, K. L. Near-field optical transducer for nanomechanical resonators. *Appl. Phys. Lett.* **2010**, *97*, 253114.
(31) Lin, Q.; Rosenberg, J.; Jiang, X.; Vahala, K. J.; Painter, O. Mechanical oscillation and cooling actuated by the optical gradient force. *Phys. Rev. Lett.* **2009**, *103*, 103601.
(32) This approximation can be obtained by considering the scattering from the N individual NEMS resonators, which make up the array. The approximation is valid if the scattered power from each resonator is a small fraction of the incident power on it. Then, the optical transmission T for the array can be expressed as a linear sum of individual interactions, resulting in a factor of $1/N$.
(33) For both of the modes, the resonance frequencies are fitted using the Euler-Bernoulli formalism with an effective undercut.
(34) Incropera, F. P.; DeWitt, D. P. *Introduction to Heat Transfer*; Wiley: New York, 1985.
(35) Ekinci, K. L.; Yakhot, V.; Rajauria, S.; Colosqui, C.; Karabacak, D. M. High-frequency nanofluidics: a universal formulation of the fluid dynamics of mems and nems. *Lab Chip* **2010**, *10*, 3013−3025.
(36) Wang, X.; Liu, C. Multifunctional Probe Array for Nano Patterning and Imaging. *Nano Lett.* **2005**, *5*, 1867−1872.
(37) Lee, M. C. M.; Wu, M. C. Tunable coupling regimes of silicon microdisk resonators using mems actuators. *Opt. Express* **2006**, *14*, 4703.
(38) Little, B. E.; Chu, S. T.; Pan, W.; Ripin, D.; Kaneko, T.; Kokubun, Y.; Ippen, E. Vertically coupled glass microring resonator channel dropping filters. *IEEE Photon. Technol. Lett.* **1999**, *11*, 215.
(39) Calleja, M.; Tamayo, J.; Nordstrom, M.; Boisen, A. Low-noise polymeric nanomechanical biosensors. *Appl. Phys. Lett.* **2006**, *88*, 113901−3.